

# Chinese NO<sub>x</sub> emission reductions and rebound as a result of the COVID-19 crisis quantified through inversion of TROPOMI NO<sub>2</sub> observations

J.Ding<sup>1</sup>, R.J. van der A<sup>1,2</sup>, H.J. Eskes<sup>1</sup>, B. Mijling<sup>1</sup>, T. Stavrakou<sup>3</sup>, J.H.G.M. van Geffen<sup>1</sup>, J.P. Veefkind<sup>1,4</sup>

<sup>1</sup> Royal Netherlands Meteorological Institute (KNMI), Utrechtseweg 297, 3731 GA De Bilt, The Netherlands.

<sup>2</sup> Nanjing University of Information Science & Technology (NUIST), Ningliu Road 219, Nanjing, P.R. China.

<sup>3</sup> Royal Belgian Institute for Space Aeronomy (BIRA-IASB), Avenue Circulaire 3, 1180 Brussels, Belgium.

<sup>4</sup> Delft University of Technology, Stevinweg 1, 2628 CN Delft, The Netherlands

Corresponding author: Jieying Ding ([jieying.ding@knmi.nl](mailto:jieying.ding@knmi.nl))

## Key Points:

- NO<sub>x</sub> emissions derived from TROPOMI observations show reductions for individual Chinese cities of about 35% due to the COVID-19 lockdown.
- Emissions of coal power plants and maritime transport show strong reductions (25-40%) during the lockdown.
- Urban emissions rebound in March to levels before the lockdown, while emissions of power plants and maritime transport take longer to recover.

## Abstract

During the COVID-19 lockdown in China low air pollution levels were reported as a consequence of the reduced economic and social activities. Quantification of the pollution reduction is not straightforward due to effects of transport, meteorology, and chemistry. Here we have analysed the NO<sub>x</sub> emission reductions calculated with an inverse algorithm applied to daily NO<sub>2</sub> observations from the TROPOMI instrument onboard the Copernicus Sentinel-5P satellite. This method allows quantification of emission reductions per city, and the analysis of emissions of maritime transport and of the energy sector separately. The reductions we found are 20 to 50% for cities, about 40% for power plants and 15 to 40% for maritime transport depending on the region. The reduction in both emissions and concentrations shows a similar timeline consisting of a sharp reduction around the Spring festival and a slow recovery from mid-February to mid-March.

## Plain Language Summary

During the COVID-19 lockdown in China, air quality had strongly improved. Here we study what sources were reduced and how much the reduction per city was. We used TROPOMI observations of the Sentinel-5P satellite, which monitors the Earth's atmosphere daily. We focused on observations of the pollutant 'nitrogen dioxide', an important pre-cursor of air pollution in the atmosphere. With our novel methodology we are able to calculate the pollution back to the sources of the emissions, whether these are big cities, industrial regions, power plants or busy shipping lanes. We applied this method to East China, where the 36 biggest Chinese cities are located. Almost all those cities showed strong emission reductions of 20-50% during the lockdown in February 2020. Besides urban China, we found an average emission reduction of 40% over coal power plants, and a reduction in maritime transport by 15-40% depending on the region. The period of reduced emissions lasted until around the end of February and the emissions slowly returned to normal during the month March 2020. Exception is the region Wuhan, the centre of the COVID-19 crisis, where emissions started to rebound since 8 April, the end of their lockdown period.

## 1 Introduction

The year 2020 is an unprecedented year, with the novel coronavirus, causing the COVID-19 disease spreading over the whole world, infecting millions of people and causing hundreds of thousands of fatalities (WHO, 2020). On 11 March 2020, the World Health Organization (WHO) qualified the spread of COVID-19 as a pandemic. To prevent the spread of the disease, many affected countries implemented COVID-19 regulations such as social distancing, teleworking and the closure of non-essential businesses. China, the first country facing the outbreak of COVID-19, enacted a lockdown from 24 January to 20 March 2020 in the Hubei province where the first cases were reported from its capital Wuhan, while other provinces limited all outdoor activities since the Chinese New Year and gradually resumed the work after 10 February (Tian et al., 2020; Wang et al., 2020).

The strict COVID-19 regulations lead to a reduction of road and air traffic, a temporary closing of companies and a decrease of industrial productivity. These in consequence affect emissions of air pollutants, especially from the transport and industry sectors, which are

significant sources of  $\text{NO}_x$  ( $\text{NO}_x = \text{NO}_2 + \text{NO}$ ) in cities. Several studies presented a large decrease of  $\text{NO}_2$  concentration during the lockdown period in China from both in-situ and satellite observations (Wang et al., 2020; Huang., 2020). Tropospheric  $\text{NO}_2$  column concentrations observed by the TROPOMI (TROPOspheric Monitoring Instrument) on the Sentinel-5P satellite decrease about 35% over China and some areas up to 60% during the COVID-19 regulation period compared to the same period of 2019 (Bauwens et al, 2020; Zhang et al., 2020). In March 2020, after the resumption of work and the gradual lifting of the lockdown restrictions, the  $\text{NO}_2$  concentrations quickly increased to similar levels as in the previous year (Bauwens et al., 2020). Because  $\text{NO}_2$  concentrations are affected by meteorology, chemistry and transport, large concentration variations are expected from day to day. Therefore the concentrations alone provide only an indication of the impact of the COVID-19 measures on air pollution. Bottom-up inventories are usually updated with few years delay due to the complexity of gathering all statistic information on source sector, land-use and sector-specific emission factors. A top-down approach using satellite observations has been demonstrated to be able to accurately and quickly provide emission estimates (Stavrakou et al., 2013; Miyazaki et al. 2020). Here we derived the  $\text{NO}_x$  emissions by using the satellite observations and a chemistry-transport model (CTM). The model is driven by meteorological analyses, accounting for the weather-related variability. The high spatial resolution of the TROPOMI observations and the inverse modelling system allows us to quantify the impact of the COVID-19 measures and distinguish emissions from cities, power plants and maritime transport separately. Recently,  $\text{NO}_x$  emissions derived from the high resolution  $\text{NO}_2$  observations of TROPOMI have been reported by Goldberg et al. (2019) and van der A et al. (2020).

To this purpose, we use the DECSO (Daily Emission estimates Constrained by Satellite Observations) algorithm, which has demonstrated its skill to capture emission changes in a short time period at city level (Mijling and van der A, 2012; Ding et al., 2015). This study presents  $\text{NO}_x$  emissions estimated from Sentinel-5P TROPOMI observations from 2019 to April 2020 over East Asia. The high spatial resolution satellite observations and daily global coverage allow us to monitor fast emission changes per city due to the implementation and to the relaxing of COVID-19 regulations.

## 2 Methodology

### 2.1 $\text{NO}_2$ observations by TROPOMI

The Copernicus Sentinel-5P satellite carries the TROPOMI instrument (Veefkind et al, 2012). TROPOMI is a spectrometer combining a high spectral resolution with high spatial resolution ( $3.5 \times 5.5 \text{ km}^2$  at nadir for the  $\text{NO}_2$  observations), high signal-to-noise ratios and a daily global coverage. Despite the much smaller footprints, the spectral fits of the individual TROPOMI ground pixels have 30% smaller noise than those from the Ozone Monitoring Instrument (OMI) and the average values agree well to within 5% (van Geffen et al, 2020).

A major difference in the retrieval of the tropospheric vertical column compared to OMI is the retrieval of the effective cloud pressure, derived from the  $\text{O}_2\text{-A}$  band in the near infrared with the FRESCO algorithm for TROPOMI, and from the  $\text{O}_2\text{-O}_2$  absorption band in OMI. The currently available TROPOMI product (versions 1.2 and 1.3) has tropospheric column which are

about 20% lower than OMI over Eastern China, and this is largely attributed to the cloud pressure retrieval difference (van Geffen et al., 2019). In the relative comparisons discussed in this paper (e.g. 2020 versus 2019) we expect a large part of such a multiplicative bias to cancel out.

The TROPOMI tropospheric NO<sub>2</sub> columns are pre-processed into “super-observations”, representing the integrated average of the TROPOMI observations over the 0.25° x 0.25° grid cells of the model after filtering for clouds. A super-observation may contain up to 25 individual observations of TROPOMI. The super-observation error takes into account spatial correlations between individual TROPOMI observations as well as representativity errors in the case of incomplete coverage. Averaging kernels are also computed for these super-observations, and are used in the emission estimates described below. This has the advantage that the assimilation result becomes independent of the coarser-resolution of the a priori profile used in the retrieval of the tropospheric column.

Figure 1 shows the mean TROPOMI NO<sub>2</sub> tropospheric column observations gridded on a 0.02° by 0.02° grid for the periods 8-28 February 2020 compared with 18 February to 4 March 2019, both after the Chinese New Year holidays. Very prominent concentration reductions are observed in February 2020 compared to 2019.

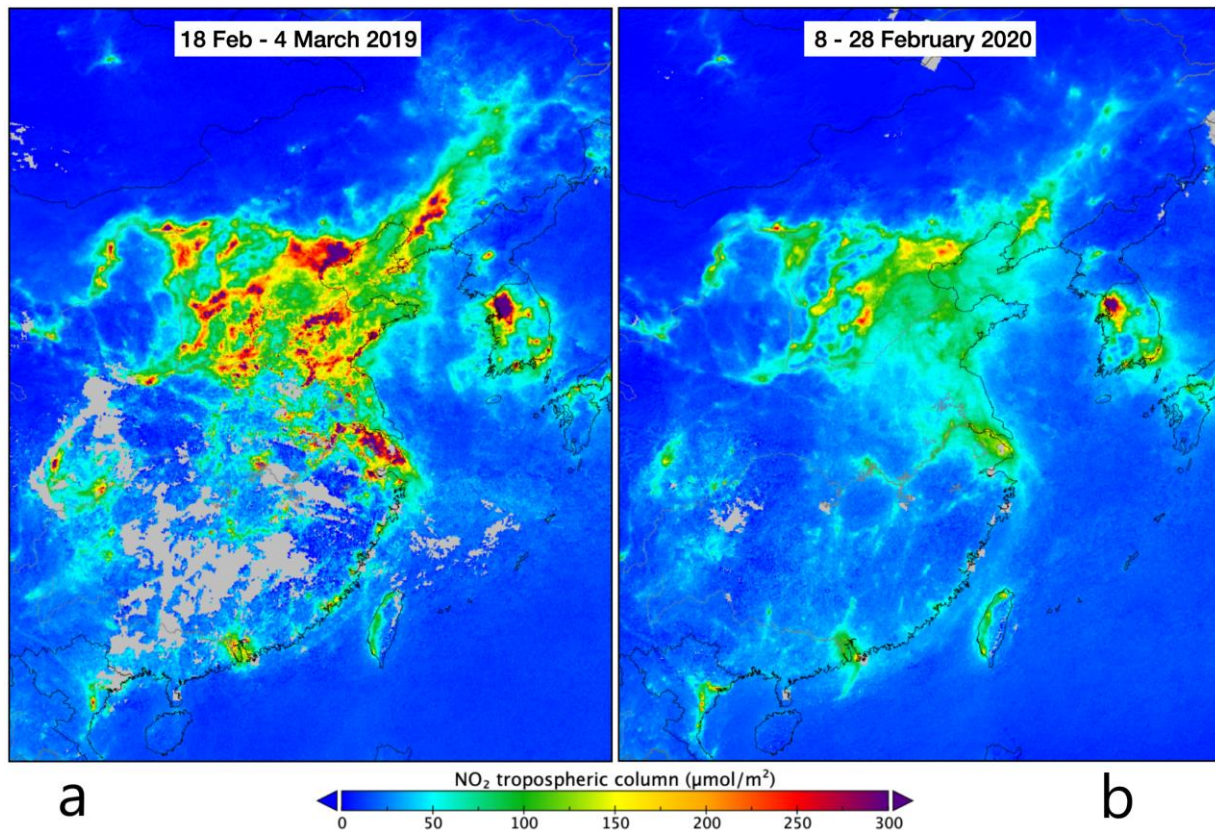


**Figure 1.** TROPOMI NO<sub>2</sub> columns over East China after the Chinese New Year in 2019 (a) and 2020 (b).

## 2.2 NO<sub>x</sub> emissions from DECSO

DECSO is a state-of-the-art inverse algorithm developed by Mijling and van der A (2012) to update daily emissions of short-lived atmospheric constituents using an extended Kalman filter, in which emissions are translated to concentrations via a CTM and compared to the satellite observations. The sensitivity of concentrations to emissions is calculated from a trajectory analysis to account for transport of the short-lived gas by using a single CTM forward run. DECSO has been successfully applied to NO<sub>2</sub> observations from OMI and TROPOMI over different regions ([www.globemission.eu](http://www.globemission.eu)). In this study, daily NO<sub>x</sub> emissions from 2019 to April 2020 over East Asia (102–120°E, 18–50°N) are derived with DECSO by using the Eulerian regional off-line CTM CHIMERE v2013 (Menut et al., 2013) and TROPOMI NO<sub>2</sub> observations. The implementation of CHIMERE v2013 in DECSO is described in Ding et al. (2015). The latest development and validation of DECSO are presented in previous studies (Ding et al., 2017; van der A et al., 2020). The novelty in our current approach is that we applied DECSO to the super-observations of TROPOMI instead of directly using individual TROPOMI observations.

## 2.3 In-situ observations

More than 1500 in-situ stations covering all major cities in China are operated by the China National Environmental Monitoring Center. They provide hourly observations of the pollutants PM<sub>10</sub>, PM<sub>2.5</sub>, O<sub>3</sub>, NO<sub>2</sub>, SO<sub>2</sub>, and CO (Bai et al., 2020). NO<sub>2</sub> is measured by a chemiluminescence technique (Zhang & Zhao, 2015). Data can be accessed via web-sites of third parties, such as [www.pm25.in](http://www.pm25.in) and [www.aqicn.org](http://www.aqicn.org). For this study we have averaged the various in-situ NO<sub>2</sub> observations in a city to a single value per hour for each of 36 selected major cities. For comparison with model results, we calculated a daily value based on the observations from 10:00 to 18:00 local time. The daytime selection is due to large inaccuracies in simulations of the nighttime boundary layer height.

## 2.4 Ensemble modelling

An operational multi-model forecasting system for air quality has been developed to provide air quality services for urban areas of China (Brasseur et al., 2019, Petersen et al., 2019). This system has been conceived and developed in the framework of two EU-funded FP-7 projects: MarcoPolo and PANDA. The ensemble model system includes nine global and regional chemistry-transport models from different research institutes from Europe and China. The ensemble service has a typical resolution of about 20 km. It provides daily forecasts of ozone, nitrogen oxides, and particulate matter for the 36 largest urban areas of East China (i.e. population higher than 3 million according to the census of 2010). These individual 3-day forecasts as well as the mean and median concentrations are publicly accessible (<http://www.marcopolo-panda.eu>). The emission inventories used as input to the models of the

ensemble do not account for the Chinese New Year or the COVID-19 lock down period. Therefore, the ensemble model represents the business-as-usual scenario.

### 3 NO<sub>x</sub> emissions reductions

NO<sub>x</sub> emissions have been affected since the strict regulations started in China, especially in the Hubei Province. We select three periods to quantify the impact of the COVID-19 regulations. The first period (P1) is three weeks before the implementation of the COVID-19 regulations, 3 to 23 January in 2020, which is also just before the Chinese New Year. The second period (P2) is 8 to 28 February, which is regarded as the regulation period. The third period (P3) is from 18 March to 7 April, when most regions in China resumed working. Figure 2 shows the relative changes of emissions during the selected 3 periods over the grid cells with high anthropogenic (above 3kg N/km<sup>2</sup>/day) NO<sub>x</sub> emissions. We observe a strong decrease of NO<sub>x</sub> emissions over China in P2 compared to P1 (Figure S1 shows the emission changes on provincial level). A few grid cells with increased emissions often coincide with industrial areas. In P3, NO<sub>x</sub> emissions increased compared to P2 but are still lower than in P1 because of the step-wise resumption of work and social life. The NO<sub>x</sub> emissions in South Korea are not significantly changed in P2 compared to the changes in China during the three periods (Figure S1), because South Korea adopted less restrictive COVID-19 regulations, mostly on voluntary basis (Bauwens et al., 2020). The emissions due to sea-transport from Shanghai to Guangzhou are less affected than the transport over land and are found to decrease by about 25% in P2 and increase again with 18% in P3 in comparison to P2. A more significant emission decline was found in the Yellow Sea and Bohai area, where NO<sub>x</sub> emissions reduced by about 41% in P2 and continued decreasing by 6% in P3.

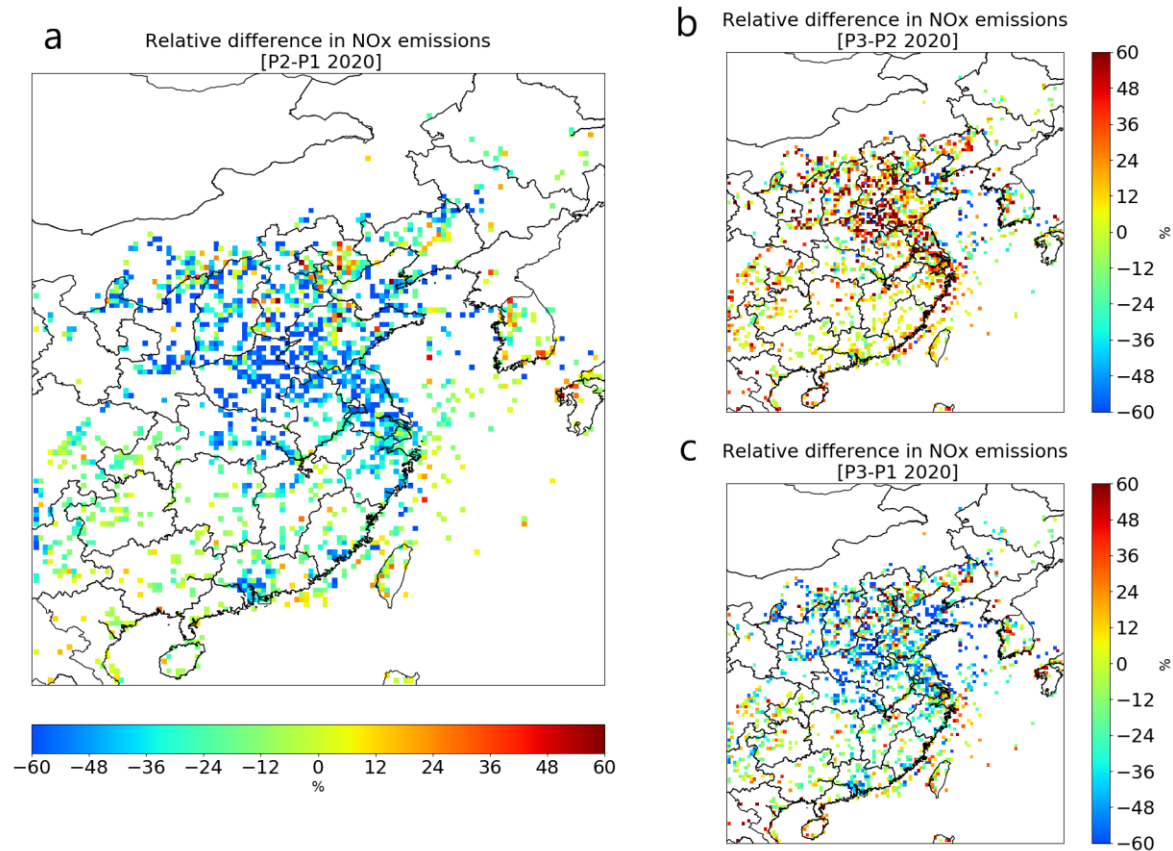


**Figure 2.** The relative difference in NO<sub>x</sub> emissions between (a) P2 and P1; (b) P3 and P2 (c) P3 and P1. P1 is 3-23 January. P2 is 8-28 February. P3 is 18 March to 7 April. The changes in emissions are shown in the figure for emissions higher than 3 kg(N)/km<sup>2</sup>/day in P1.

At city level changes in NO<sub>x</sub> emissions started from January 2019. Figure 3 shows the time series of emissions at 6 large cities in China and in Seoul, the capital of South Korea. We infer a very strong NO<sub>x</sub> emission decrease of more than 50% during and after the 2020 Chinese New Year in Wuhan, where the COVID-19 outbreak was first recorded and very strict lockdown regulations were adopted, while an almost negligible reduction in NO<sub>x</sub> emissions is derived during the 2019 Chinese New Year. At the other five Chinese cities, we also observe a much stronger decrease after the Chinese New Year in 2020 than in 2019. In addition, the duration of the period with low emissions is much longer. Most cities in China display a stronger decrease in 2020 (see Table S1), which is attributed to the COVID-19 measures. The averaged NO<sub>x</sub> emission reduction at the selected cities shown in table S1 is 35%. We also calculate the average reduction of grid cells containing urban areas selected by using the land-use data of the GlobCover Land Cover dataset. The inferred emission reduction is about 35% in urban areas, which is the same as the average reduction in the selected cities. Note that the NO<sub>x</sub> emissions are usually lower by about 10% during the Chinese New Year with less business and industrial activities (Ding et al., 2017). The time line of NO<sub>x</sub> emissions in Beijing show a slightly different pattern with a relatively low reduction during the COVID-19 lockdown, but already strong emission reductions during the politically important “two-sessions” meeting in March 2019 and

especially the celebration of 70<sup>th</sup> national anniversary of China around 1 October 2019, when many factories were closed and strict emission regulations were enforced (Yang et al., 2020). Figure 3 also shows that the NO<sub>x</sub> emissions start to increase again in March, in line with the step-by-step recovery of the human activities. Except for Wuhan with the emission rebound after 8 April, when the lockdown was lifted, by the end of March all cities reached a level of NO<sub>x</sub> emissions close to what was observed in the same period in 2019. This is consistent with the economic target of China. It has been reported that China has a temporary economic setback due to the COVID-19 outbreak, but will accelerate the return to the pre-crisis economic level (e.g. Ouyang, 2020).

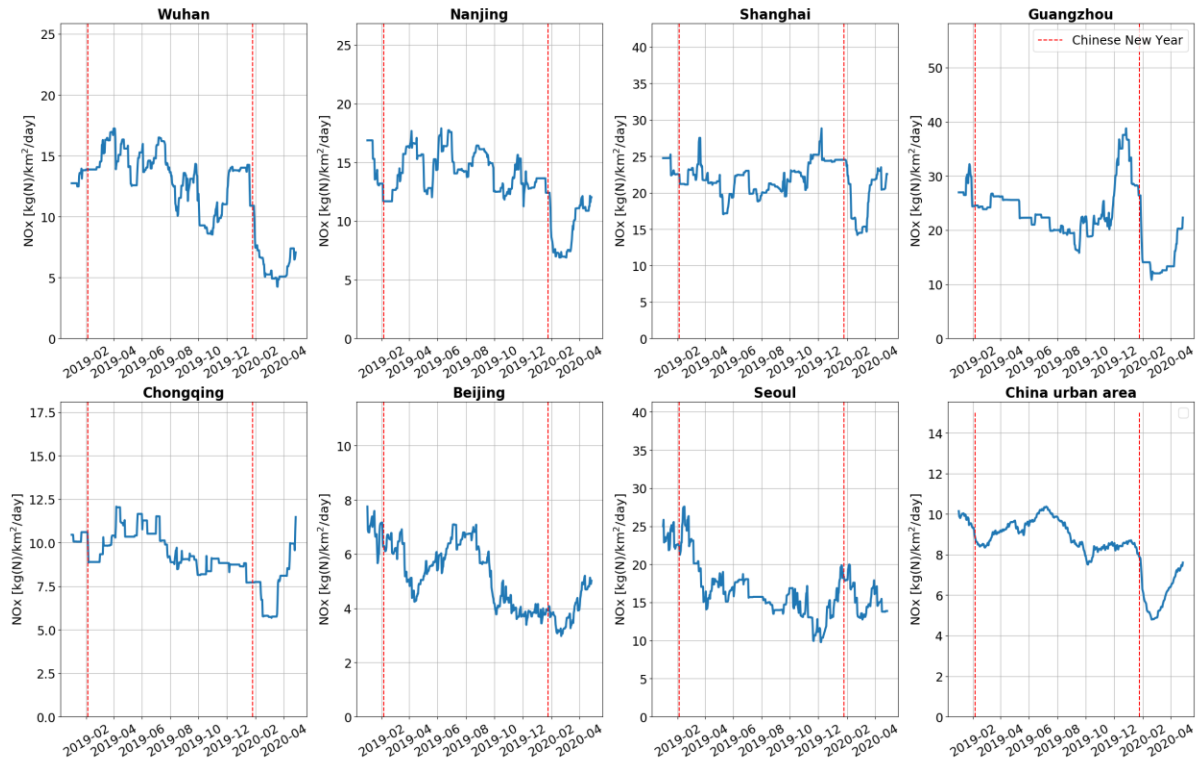


**Figure 3.** Time series (1 January 2019 to 28 April 2020) of daily NO<sub>x</sub> emissions in 7 cities and urban China. The red dashed lines indicate the Chinese New Year in 2019 and 2020. 6 Chinese cities are considered (Wuhan, Nanjing, Shanghai, Guangzhou, Chongqing and Beijing) as well as Seoul.

Besides the urban emissions, we find strong reductions of NO<sub>x</sub> emissions from coal power plants. Figure 4 shows time series of NO<sub>x</sub> emissions from the Ningxia Province, where the main sources of NO<sub>x</sub> are fossil fuel power plants (van der A et al., 2017). Ningxia province can serve as an indication of the national energy production by coal power plants. It has a population of about 6 millions, only 0.4% of the total population of China. Its coal production and electricity generation from coal power plants are in the top ten list of provinces and about 80% of the generated energy is consumed by the industry (Ningxia Statistics Bureau, 2019). Our inversion results indicate that after the 2020 Chinese New Year, NO<sub>x</sub> emissions dropped about 40% in this

province, 20% more than in 2019 New Year period. This shows the impact of the COVID-19 regulations on the energy production, especially in the industrial sector. According to the National Bureau of Statistics of China (2020), the total profit of the first three months in 2020 made by industrial enterprises decreased around 40% in China compared to the same period of the previous year. The shrinking of the industrial economy results in lower energy consumption, which is clearly reflected by the decrease of  $\text{NO}_x$  emissions from power plants.

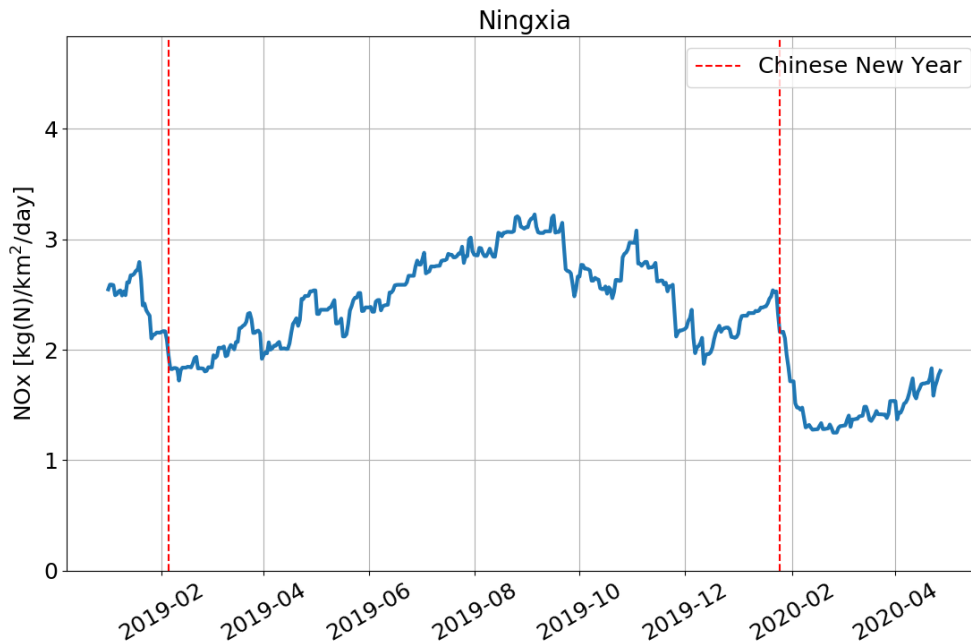
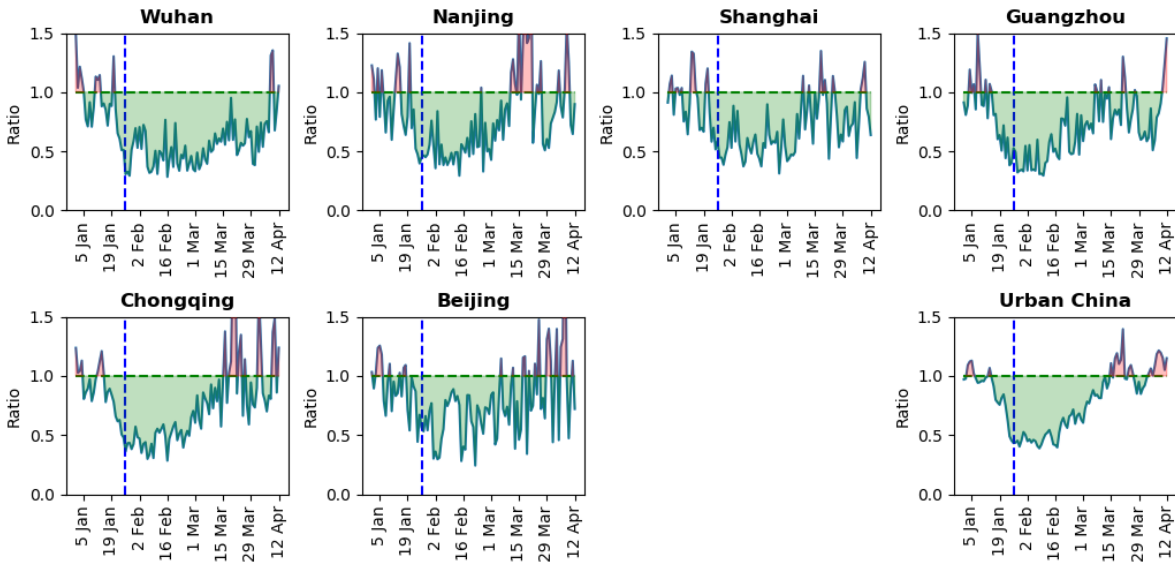


**Figure 4.** Time series (1 January 2019 to 28 April 2020) of daily  $\text{NO}_x$  emissions in Ningxia Province. The red dashed lines indicate the Chinese New Year in 2019 and 2020.

#### 4 Concentration reductions

Although the  $\text{NO}_2$  concentrations at the surface are affected by transport, meteorology and chemical lifetime, more or less similar reductions are to be expected for the total column. To eliminate the effect of meteorology and transport we compare the measurements of in-situ stations with the MarcoPolo-Panda ensemble model driven by emission inventories (business-as-usual model), which are not corrected for the effects of either Spring Festival or the COVID-19 crisis. A possible bias between measurements and model is corrected for by normalizing the results for the first two weeks of January. In Figure 5 the ratio between in-situ measured  $\text{NO}_2$  and the modelled  $\text{NO}_2$  is shown. The concentration reductions are shown as green area, while increased concentrations are shown in red. The reduction starts around the Chinese New Year and ends in March. Exception is the concentration level of Wuhan that becomes similar to that of the business-as-usual scenario after the first week of April. Table S1 shows the concentration reduction in P2 compared to P1 for the selected 36 cities. The average concentration reduction is 41%, while for emissions the reduction is 35%. A striking difference between Wuhan and the other Chinese cities is the longer duration (by about one month) of the concentration reductions.

267



268

269

270

271

272

273

274

275

276

277

278

279

280

281

282

283

284

285

286

287

288

289

290

291

292

293

294

295

296

**Figure 5.** Measured  $\text{NO}_2$  concentrations (from 1 January to 12 April 2020) compared to concentrations of the business-as-usual scenario. Cities are chosen similar to Figure 3, except for Seoul. The Chinese New Year is indicated by the blue dashed line.

## 5 Conclusions

To study the impact of the COVID-19 regulations on  $\text{NO}_x$  emissions (one of the key ingredients determining air pollution), we derived daily  $\text{NO}_x$  emissions at a resolution of  $0.25^\circ \times 0.25^\circ$  over East Asia from 2019 to March 2020 by applying the inverse algorithm DECSO to observations from TROPOMI. By grouping the emission into three periods of before, during and after the COVID-19 regulations, we quantified the emission changes on the small spatial scale of city level and from different emission sources such as sea-transport and the energy sector. The observations suggest emission reductions of 20% to 50% for cities. The emissions reduction of 40% in the Ningxia province reflects the impact of the lockdown measures on the energy sector. Maritime transport is also affected during the COVID-19 regulations, although its emissions reductions are dependent on the region. Along the ship track from Shanghai to Guangzhou, the  $\text{NO}_x$  emissions decreased by 25% during the lockdown and increased again by 18% after the work resumption. While in the region of the Yellow sea and Bohai sea, the emissions decrease by 40% and continued decreasing with another 6% also in March. To further analyze the impact of emission reductions, we compared the in situ  $\text{NO}_2$  concentration measurements with simulated surface concentrations from models using unaltered emissions. The emission reductions follow a similar timeline as the surface  $\text{NO}_2$  concentrations, which show a sharp reduction around the Chinese New Year and a slow recovery from mid-February to mid-March. Wuhan, the city of the epicenter of the COVID-19 crisis, shows large emission reductions in both February and March, reaching nominal levels in April. In general, we found that activities in the cities returned to normal in March, while as an indicator of the economy, emissions of energy production and international maritime transport, took a longer time to return to pre-COVID-19 levels (Table S2).

With the  $\text{NO}_x$  emissions derived from DECSO using observations from TROPOMI, we are able to get detailed information about the impact on emission changes due to the COVID-19

regulations by accounting for the influence of meteorology, lifetime and transport of the air pollutants. As the COVID-19 crisis progressively affects all continents, the public health regulations implemented by various countries may have different contributions to air quality. Applying our methodology to different regions can help to quantify the impact of the NO<sub>x</sub> emission reductions by the different regulations on not only the improvement of air quality from urban to local to regional scale.

### Acknowledgments, Samples, and Data

This research has been supported by the project “Impact study of COVID-19 lockdown measures on air quality and climate” (2020) of the European Space Agency. This publication contains modified Copernicus Sentinel-5P data 2019-2020. TROPOMI data version 1.2.2 and 1.3.0 used is available at <https://s5phub.copernicus.eu/>. We acknowledge the ESA GlobCover 2009 project for the land use data set on [http://due.esrin.esa.int/page\\_globcover.php](http://due.esrin.esa.int/page_globcover.php). The NO<sub>x</sub> emissions dataset in this study is available on [www.globemission.eu](http://www.globemission.eu).

### References

Bai, K., Li, K., Guo, J., Yang, Y., Chang, N.-B. (2020). Filling the gaps of in situ hourly PM<sub>2.5</sub> concentration data with the aid of empirical orthogonal function analysis constrained by diurnal cycles. *Atmospheric Measurement Techniques*, 13, 3, 1213-1226, DOI: 10.5194/amt-13-1213-2020.

Bauwens, M., Compernelle, S., Stavrou, T., Müller, J.-F., van Gent, J., Eskes, H., et al. (2020). Impact of coronavirus outbreak on NO<sub>2</sub> pollution assessed using TROPOMI and OMI observations. *Geophysical Research Letters*, <https://doi.org/10.1029/2020GL087978>, 2020

Brasseur, G. P., Xie, Y., Petersen, A. K., Bouarar, I., Flemming, J., Gauss, M., et al. (2019). Ensemble forecasts of air quality in eastern China - Part 1: Model description and implementation of the MarcoPolo-Panda prediction system, version 1, *Geosci. Model Dev.*, 12, 33-67, <https://doi.org/10.5194/gmd-12-33-2019>.

Ding, J., van der A, R. J., Mijling, B., Levelt, P. F., & Hao, N. (2015). NO<sub>x</sub> emission estimates during the 2014 Youth Olympic Games in Nanjing. *Atmos. Chem. Phys.*, 15(16), 9399-9412. doi:10.5194/acp-15-9399-2015

Ding, J., Miyazaki, K., van der A, R. J., Mijling, B., Kurokawa, J. I., et al. (2017). Intercomparison of NO<sub>x</sub> emission inventories over East Asia. *Atmos. Chem. Phys.*, 17(16), 10125-10141. doi:10.5194/acp-17-10125-2017

Goldberg, D., L., Lu, Z., Streets, D., G., de Foy, B., Griffin, D., McLinden, C., A., et al. (2019). Enhanced Capabilities of TROPOMI NO<sub>2</sub>: Estimating NO<sub>x</sub> from North American Cities and

Power Plants, *Environ. Sci. Technol.*, 53, 21, 12594-12601,  
<https://doi.org/10.1021/acs.est.9b04488>.

Gu, J., Chen, L., Yu, C., Li, S., Tao, J., Fan, M., et al. (2017) Ground-Level NO<sub>2</sub> Concentrations over China Inferred from the Satellite OMI and CMAQ Model Simulations. *Remote Sens.*, 9(6), 519, <https://doi.org/10.3390/rs9060519>

Huang, X., Ding, A., Gao, J., Zheng, B., Zhou, D., et al. (2020). Enhanced secondary pollution offset reduction of primary emissions during COVID-19 lockdown in China. *EarthArXiv.*, April 13. <https://doi.org/10.31223/osf.io/hvuzy>

Menut, L., Bessagnet, B., Khvorostyanov, D., Beekmann, M., Blond, N., Colette, A., et al. (2013). CHIMERE 2013: A model for regional atmospheric composition modelling. *Geoscientific Model Development*, 6(4), 981–1028. <https://doi.org/10.5194/gmd-6-981-2013>

Mijling, B., and van der A, R. J. (2012). Using daily satellite observations to estimate emissions of short-lived air pollutants on a mesoscopic scale. *Journal of Geophysical Research: Atmospheres*, 117(D17). doi:10.1029/2012JD017817

Miyazaki, K., Bowman, K., Sekiya, T., Eskes, H., Boersma, F., Worden, H., et al. (2020). An updated tropospheric chemistry reanalysis and emission estimates, TCR-2, for 2005–2018, *Earth Syst. Sci. Data Discuss.*, <https://doi.org/10.5194/essd-2020-30>, in review.

National Bureau of Statistics of China (2020). Available online: [http://www.stats.gov.cn/english/PressRelease/202004/t20200428\\_1742015.html](http://www.stats.gov.cn/english/PressRelease/202004/t20200428_1742015.html) (last access date: 3 May 2020)

Ningxia Statistics Bureau (2019). The Achievements of Economic and Social Development during the last 70 years, part 3, in Chinese. Available online: [http://tj.nx.gov.cn/tjxx/201909/t20190923\\_1750612.html](http://tj.nx.gov.cn/tjxx/201909/t20190923_1750612.html) (last access date: 9 May 2020)

Ouyang S. (2020). COVID-19 will not alter China's growth story, top economic regulator says, *China Daily*. Available online: <https://global.chinadaily.com.cn/a/202004/20/WS5e9d51f8a3105d50a3d1779c.html> (last access date: 27 April 2020)

Petersen, A. K., Brasseur, G. P., Bouarar, I., Flemming, J., Gauss, M., Jiang, F., et al (2019). Ensemble forecasts of air quality in eastern China - Part 2: Evaluation of the MarcoPolo-Panda

prediction system, version 1. *Geosci. Model Dev.* 12, 1241-1266, <https://doi.org/10.5194/gmd-12-1241-2019>.

Shindell, D. T., Faluvegi, G., Koch, D. M., Schmidt, G. A., Unger, N., & Bauer, S. E. (2009). Improved Attribution of Climate Forcing to Emissions. *Science*. 326(5953), 716-718. doi:10.1126/science.1174760

Stavrou, T., Müller, J.-F., Boersma, K. F., van der A, R. J., Kurokawa, J., Ohara, T., and Zhang, Q. (2013). Key chemical NO<sub>x</sub> sink uncertainties and how they influence top-down emissions of nitrogen oxides, *Atmos. Chem. Phys.*, 13, 9057–9082, <https://doi.org/10.5194/acp-13-9057-2013>.

Tian, H., Liu, Y., Li, Y., Wu, C.-H., Chen, B., Kraemer, M. U. G., et al. (2020). An investigation of transmission control measures during the first 50 days of the COVID-19 epidemic in China. *Science*, eabb6105. doi:10.1126/science.abb6105

van der A, R. J., Mijling, B., Ding, J., Koukouli, M. E., Liu, F., Li, Q., et al. (2017). Cleaning up the air: effectiveness of air quality policy for SO<sub>2</sub> and NO<sub>x</sub> emissions in China. *Atmos. Chem. Phys.*, 17(3), 1775-1789. doi:10.5194/acp-17-1775-2017

van der A, R. J., de Laat, A. T. J., Ding, J., & Eskes, H. J. (2020). Connecting the dots: NO<sub>x</sub> emissions along a West Siberian natural gas pipeline. *npj Climate and Atmospheric Science*, 3(1), 16. doi:10.1038/s41612-020-0119-z

van Geffen, J., Boersma, K. F., Eskes, H., Sneep, M., ter Linden, M., Zara, M., and Veefkind, J. P.: S5P TROPOMI NO<sub>2</sub> slant column retrieval: method, stability, uncertainties and comparisons with OMI, *Atmos. Meas. Tech.*, 13, 1315–1335, <https://doi.org/10.5194/amt-13-1315-2020>, 2020.

van Geffen, J. H. G. M., Eskes, H. J., Boersma, K. F., Maasakkers, J. D., and Veefkind, J. P. (2019). TROPOMI ATBD of the total and tropospheric NO<sub>2</sub> data products, Report S5P-KNMI-L2-0005-RP, version 1.4.0, released 6 February 2019, KNMI, De Bilt, the Netherlands, available at: <http://www.tropomi.eu/documents/atbd/>, last access: 17 March 2020.

Veefkind, J. P., Aben, I., McMullan, K., Förster, H., de Vries, J., Otter, G., et. al. (2012). TROPOMI on the ESA Sentinel-5 Precursor: A GMES mission for global observations of the atmospheric composition for climate, air quality and ozone layer applications. *Remote Sensing of Environment*, 120, 70-83. doi:<https://doi.org/10.1016/j.rse.2011.09.027>

- Wang, P., Chen, K., Zhu, S., Wang, P., & Zhang, H. (2020). Severe air pollution events not avoided by reduced anthropogenic activities during COVID-19 outbreak. *Resources, Conservation and Recycling*, 158, 104814. doi:<https://doi.org/10.1016/j.resconrec.2020.104814>
- WHO (2020). The World Health Organization. Coronavirus Disease (COVID-19) Pandemic. Available online: <https://www.who.int/emergencies/diseases/novel-coronavirus-2019> (last access date: 27 April 2020)
- Yang, Y., Wang, Y., Yao, D., Zhao, S., Yang, S., et al. (2020). Significant decreases in the volatile organic compound concentration, atmospheric oxidation capacity and photochemical reactivity during the National Day holiday over a suburban site in the North China Plain, *Environmental Pollution*, Volume 263, Part A, 114657, <https://doi.org/10.1016/j.envpol.2020.114657>.
- Zhang, R., Zhang, Y., Lin, H., Feng, X., Fu, T.-M., & Wang, Y. (2020). NO<sub>x</sub> Emission Reduction and Recovery during COVID-19 in East China. *Atmosphere*, 11(4), 433
- Zhang, Y., Cao, F. (2015) Fine particulate matter (PM<sub>2.5</sub>) in China at a city level. *Sci Rep* 5, 14884. <https://doi.org/10.1038/srep14884>